Open access • Journal Article • DOI:10.1002/ANIE.201911419

Hybrid Metal Halides with Multiple Photoluminescence Centers — Source link

Mingze Li, Jun Zhou, Guojun Zhou, Maxim S. Molokeev ...+7 more authors

Institutions: University of Science and Technology Beijing, Siberian Federal University, Swiss Federal Laboratories for Materials Science and Technology, ETH Zurich ...+1 more institutions

Published on: 16 Dec 2019 - Angewandte Chemie (Wiley)

Topics: Halide and Photoluminescence

Hybrid Metal Halides with Multiple Photoluminescence Centers

Angewandte Chemie
GDCh
Eine Zeitschrift der Gesellschaft Deutscher Chemiker
www.angewandte.de

Akzeptierter Artikel

Titel: Hybrid Metal Halides with Multiple Photoluminescence Centers

Autoren: Zhiguo Xia, Mingze Li, Jun Zhou, Guojun Zhou, Maxim Molokeev, Jing Zhao, Viktoriia Morad, and Maksym Kovalenko

Zitierweise: *Angew. Chem. Int. Ed.* 10.1002/anie.201911419
Angew. Chem. 10.1002/ange.201911419

Link zur VoR: http://dx.doi.org/10.1002/anie.201911419
http://dx.doi.org/10.1002/ange.201911419

WILEY-VCH

10.1002/ange.201911419

WILEY-VCH

RESEARCH ARTICLE

Hybrid Metal Halides with Multiple Photoluminescence Centers

Mingze Li, Jun Zhou, Guojun Zhou, Maxim S. Molokeev, Jing Zhao, Viktoriia Morad, Maksym V. Kovalenko and Zhiguo Xia*

Abstract: Very little is known about the realm of solid-state metal halide compounds comprising simultaneously two or more halometalate anions. Such compounds would be of great interest if their optical and electronic properties could be rationally engineered, especially the synergistic effects. Here, we report the discovery of a new example of metal halide cluster-assembled compound $(C_9NH_{20})_9[Pb_3Br_{11}](MnBr_4)_2$, featuring distinctly different anionic polyhedra, namely, a rare lead halide cluster $[Pb_3Br_{11}]^{5-}$ and $[MnBr_4]^{2-}$. In accordance with its multinary zero-dimensional (0D) structure, this compound is found to contain two distinct emission centers, 565 nm and 528 nm, which are attributed to the the formation of self-trapped excitons and ^4D-$^6A_1$ transition of Mn^{2+} ions, respectively. The spectral interplay of these emission bands is governed by the excitation wavelength and temperature, and we propose a possible exchange mechanism between the two centers. Based on the high durability of $(C_9NH_{20})_9[Pb_3Br_{11}](MnBr_4)_2$ upon light and heat, as well as high photoluminescence quantum yield (PLQY) of 49.8% under 450 nm blue light excitation, white light-emitting diodes (WLEDs) are fabricated, showcasing its potential in backlight application.

White-light-emitting diodes (WLEDs) have revolutionized solid-state lighting and have also been widely used as backlighting in liquid crystal displays (LCDs) due to their superior characteristics.[1] Considering its high efficiency and low cost, a blue LED chip with a mixture of green and red phosphors becomes the mainstream of WLEDs for LCDs, and thus the blue light-excitable components are greatly demanded. Next to the conventional rare-earth doped phosphors,[2] an increasing research effort concentrates on the emerging organic-inorganic and fully inorganic hybrid metal halides as alternative narrowband and broad-band emitters, for applications ranging from WLEDs to remote thermometry.[3] However, very few luminescent metal halides can be photoexcited with blue light, which is a pre-requisite for the practical deployment in WLEDs. Hence, the discovery of such compounds with a suited optical absorption, as well as needed thermal and chemical durability, remains a formidable challenge.

It is anticipated that multi-ionic solid-state compounds containing more than one cationic or anionic species in a single phase, or mixed polyhedra therein will yield new chemical, electronic and optical functionalities, desired for applications in nonlinear optics, solar cells, and other devices.[4] Recently, low-dimensional organic-inorganic hybrid and fully inorganic halides have been extensively investigated as broadband, bright emitters in the visible spectral range.[5] To date, the photophysics of such low-dimensional metal halide is rather well established, foremost for compounds of Sn^{2+}, Sb^{3+}, Pb^{2+}, known to exhibit bright emission from the self-trapped excitons (STE) or excited-state structural reorganization (ESSR).[3d,6] Here, the description of ESSR is denoted as the photophysics process in zero-dimensional (0D) system with anionic polyhedra completely isolated from each other, which is similar as STE mentioned in corrugated-2-dimensional (2D) or 1-dimensional (1D) structure. These studies have set a stage for the exploration of materials with higher complexity. While constraining to 0D halometalate ions as building units, their mixing in one lattice is a logical next-step materials design platform.[7]

In this study we sought of building a complex material whose elementary building blocks are both luminescent and individually well understood, yet they both exploit different light-emission phenomena. As the first building block, we choose lead halide polyhedra, known for their strong electron-phonon coupling, in which STE or ESSR was considered to explain the photoluminescence (PL) mechanism, and we use STE, a more general process, to describe the as-observed PL hereafter.[8] As a second building block, tetrahedral manganese Mn^{2+} halide units are chosen for their bright green emission stemming from highly localized intra-atomic d-d transitions in Mn^{2+} ions. Tetrahalide coordination of Mn^{2+} is commonly reported to form in solutions containing bulky counterions.[9] Here, we designed a novel, solution-grown 0D metal halide that features such distinctly different Pb and Mn-containing polyhedra, $(C_9NH_{20})_9[Pb_3Br_{11}](MnBr_4)_2$. Although the synthesis conditions outlined below are similar to those we reported for structurally-related $(C_9NH_{20})_6Pb_3Br_{12}$,[10] Mn^{2+} maintains its strong inclination to form tetrahalometalate species and hence, even at small amounts of Mn^{2+}, a novel

[a] M. Z. Li†, J. Zhou†, G. J. Zhou, Prof, Dr. J. Zhao, Prof. Dr. Z. G. Xia
School of Materials Sciences and Engineering, University of Science and Technology Beijing, Beijing 100083 (P. R. China)
E-mail: xiazg@ustb.edu.cn
[†] These authors contributed equally
[b] Prof. Dr. Maxim S. Molokeev
Laboratory of Crystal Physics, Kirensky Institute of Physics, Federal Research Center KSC SB RAS, Krasnoyarsk 660036 (Russia), Siberian Federal University, Krasnoyarsk, 660041 (Russia)
Department of Physics, Far Eastern State Transport University Khabarovsk, 680021 (Russia)
[c] Prof. Dr. Z. G. Xia
State Key Laboratory of Luminescent Materials and Devices and Institute of Optical Communication Materials, South China University of Technology, Guangzhou, 510641, China
E-mail: xiazg@scut.edu.cn
[d] Viktoriia Morad, Prof, Dr. Maksym V. Kovalenko
Laboratory of Inorganic Chemistry, Department of Chemistry and Applied Bioscience, ETH Zürich, Vladimir Prelog Weg 1, CH-8093 Zürich, Switzerland,
Laboratory for Thin Films and Photovoltaics, Empa-Swiss Federal Laboratories for Materials Science and Technology, Ü berlandstrasse 129, CH-8600 Dübendorf, Switzerland
Supporting information for this article is given via a link at the end of the document.

cluster-assembled $(C_9NH_{20})_9[Pb_3Br_{11}](MnBr_4)_2$ phase is formed as a minor component next to the majority phase of Mn-free $(C_9NH_{20})_6Pb_3Br_{12}$. When the Mn-proportion is increased to two/thirds of that of Pb ions, a pure, single-phase $(C_9NH_{20})_9[Pb_3Br_{11}](MnBr_4)_2$ is obtained. This compound exhibits dual-emission, *i.e.* simultaneously from STE formed on lead-halide units and from intraatomic transitions in Mn^{2+}. The spectral behavior of these emission bands is adjustable by the temperature as well as by the excitation wavelengths. Compelling set of characteristics that include good thermal stability, high photoluminescence quantum yield (PL QY) of 49.8%, and PL excitation band in the blue region point to the promise of such multinary halides for applications in WLEDs.

Single crystals of $(C_9NH_{20})_9[Pb_3Br_{11}]$ $(MnBr_4)_2$ were prepared by slowly cooling the saturated N, N-Dimethylformamide (DMF) solution of stoichiometric quantities of the precursors to room temperature, and Figure 1a outlines this synthesis method. Yellow single crystals $(C_9NH_{20})_9[Pb_3Br_{11}](MnBr_4)_2$ with relatively large size (~ 1 cm) were obtained as shown in the optical photographs (Figure 1b). The crystal structure was determined using single crystal X-ray diffraction (SCXRD), which revealed trigonal structure with space group *P31c*. The well-fitted powder X-ray diffraction (PXRD) of simulated and experimental data (Figure 1c) show the high purity and uniformity of the as-prepared $(C_9NH_{20})_9[Pb_3Br_{11}](MnBr_4)_2$ crystals. The main crystallographic parameters are shown in Table S1 and the crystal structure and local structure descriptions are shown in Figure 1d. The crystallographic data was deposited in Cambridge Crystallographic Data Centre (CCDC # 1958545). The data can be downloaded from the site (www.ccdc.cam.ac.uk/data_request/cif). The independent part of the unit cell contains one $[PbBr_6]^{4-}$ octahedron, two $[MnBr_4]^{2-}$ tetrahedra and three C_9NH_{20} molecules. The 3-fold symmetry element multiplies $[PbBr_6]^{4-}$ into $[Pb_3Br_{11}]^{5-}$ trimer block by face-sharing. These $[Pb_3Br_{11}]^{5-}$ blocks and $[MnBr_4]^{4-}$ tetrahedra are isolated from each other and thus form a 0D type metal halide structure. During the structural determination, it is also found that some Br^- sites have large thermal parameters suggesting the presence of a vacancy or a light ion in these sites besides Br^-. Considering that the synthesis is conducted under ambient conditions, the presence of OH^- was anticipated and further confirmed by the infrared (IR) spectroscopy (Figure S1). Drying samples at 393 K for 12 h does not deteriorate the broad signal of hydroxyl groups at around 3500 cm^{-1}. The crystallographic information file (CIF) of $(C_9NH_{20})_9[Pb_3Br_{11}](MnBr_4)_2$ phase can be found in the Supporting Information (SI). Figure S2a shows the scanning electron microscope (SEM) photograph of this crystal (~ 500 μm) with well-developed crystal face, while the elemental maps in Figure S2 b-d evidence homogeneous distributions of Pb, Br, and Mn. The detailed results of energy dispersive X-ray spectroscopy (EDS, Table S2) and elemental analysis (EA, Table S3) further confirm the composition of inorganic and organic parts, respectively. Moreover, it is worth mentioning that a similar 0D metal halide $(C_9NH_{20})_9[Pb_3Cl_{11}](ZnCl_4)_2$, albeit with the different structure, had been published in the course of this work.[7b] A different structural model ($P6_3$) is obtained for $(C_9NH_{20})_9[Pb_3Cl_{11}](ZnCl_4)_2$, which is possibly related with the fact that the degrees of ordering and distortion for organic and inorganic species could be significantly different in the two compounds.

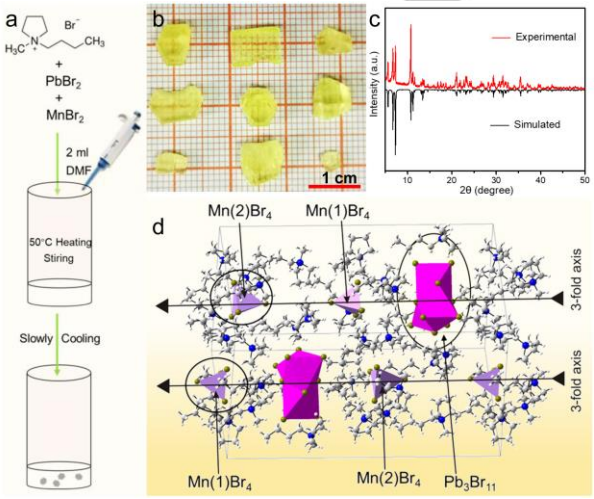

Figure 1. a) Schematic diagram showing the crystal growth of $(C_9NH_{20})_9[Pb_3Br_{11}](MnBr_4)_2$. b) Optical photographs of as-grown $(C_9NH_{20})_9[Pb_3Br_{11}](MnBr_4)_2$ crystals under daylight. c) The simulated and experimental X-ray powder patterns of $(C_9NH_{20})_9[Pb_3Br_{11}](MnBr_4)_2$. d) The asymmetric part of the $(C_9NH_{20})_9[Pb_3Br_{11}](MnBr_4)_2$ unit cell and the marked polyhedrons.

The photoluminescence excitation (PLE), PL emission spectra and decay curves at room temperature (298 K) were measured to characterize photophysical properties of $(C_9NH_{20})_9[Pb_3Br_{11}](MnBr_4)_2$ (Figure 2). Inset of Figure 2a, evidences different emission colors (yellow/green) at different excitation wavelengths, in accord with the PL spectra. In the following, the emission bands upon shorter and longer wavelength excitations are denoted as band 1 and band 2, respectively. As given in Figure 2a, the band 1 peaked at 565 nm upon 365 nm excitation with a full width at half maximum (FWHM) of 75 nm has a large Stokes shift of 200 nm, while the band 2 peaked at 528 nm upon 450 nm excitation with a FWHM of 67 nm has a smaller Stokes shift of 78 nm. Such PL variance in relation to the excitation wavelengths strongly suggests the existence of several kinds of emission centers. Thus, to understand the luminous mechanism of multiple emission centers, room-temperature decay curves monitored at 565 nm and 528 nm and excited at 365 nm and 450 nm, respectively, were acquired (Figure 2b). All luminescence decay curves can be satisfactory fitted with a single-exponential function (1):

$$I(t) = A \exp(-t/\tau) \quad (1)$$

where I is the luminescence intensity, t is the time after excitation, A is a constant and τ is lifetime for exponential component. Based on Eq.(1), the effective decay times were calculated to be 27.43 ns of band 1 and 114.26 μs of band 2. The short nanosecond lifetime for band 1 is consistent with other Pb-based halides with STE emission.

10.1002/ange.201911419

WILEY-VCH

RESEARCH ARTICLE

[6d] The long lifetime for band 2 is ascribed to ^{4}D to $^6A_1$ transition of tetrahedrally coordinated Mn^{2+} with spin-forbidden transitions. The above results also confirm the existence of two luminescence centers in $(C_9NH_{20})_9[Pb_3Br_{11}](MnBr_4)_2$. Additionally, Figure S3 and Figure S4 show decay curves at excitation wavelengths of 365 nm and 450 nm, respectively, yielding very similar PL lifetimes at different emission wavelengths, which reinforces the assignment of band 1 and band 2 to a single luminescence center. Moreover, two emission bands are clearly independent and they will not overlap when the excitation wavelength changes from 365 nm to 450 nm (Figure 3d). The CIE chromaticity coordinate for band 1 with yellow emission and band 2 with green emission are calculated to be (0.409, 0.501) and (0.293, 0.645), respectively (Figure S5). Interestingly, although the PL intensities of band 1 and band 2 are similar, the PLQY at 298 K are much lower for band 1 (15.7 %) in comparison to band 2 (49.8 %). The reason may be due to the more efficient transition process of ^{4}D to $^6A_1$ in Mn^{2+} with fewer non-radiative transitions, which is consistent with multiple reports on high PLQY in 0D-halides of Mn^{2+}.[11] On contrary, we hypothesised that STE emission is probly quenched by coupling to phonons and thus show low PLQY at room temperature. There's a lack of studies of such quenching in Pb-based systems, where spin-orbit coupling is competing with electron-phonon coupling, but is well-known in Sn, Sb systems.[3d]

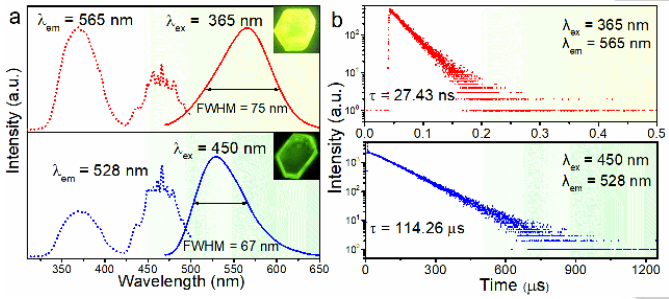

Figure 2. a) Room-temperature PL and PLE spectra of $(C_9NH_{20})_9[Pb_3Br_{11}](MnBr_4)_2$ recorded at different excitation wavelengths (365 nm and 450 nm) and emission wavelengths (565 nm and 528 nm). b) Room-temperature PL decay curves monitored at 565 nm and 528 nm and excited at 365 nm and 450 nm.

From the above spectral data, we draw the following conclusions: (1) only STE emission can be observed at room temperature for band 1, but without Mn^{2+} emission. Mn^{2+} emission quenching at room temperature has also been reported in host-dopant systems, and the back-energy transfer (BET) process, which is strongly dependent on temperature, had been proposed as the explanation for this phenomenon.[12] The sufficient thermal energy at high temperatures activates BET channel, while at low temperatures it will be significantly suppressed. (2) Conversely, only Mn^{2+} emission can be observed for band 2. This is due to the insufficient excitation energy for $[Pb_3Br_{11}]$. The electrons have enough energy to be excited to the excited stated (ES) of $[Pb_3Br_{11}]$ upon 365 nm (3.40eV) excitation, while upon 450 nm (2.76 eV) excitation, the electrons with less excitation energy can only be excited to the Mn^{2+} ^{4}G-derived states.

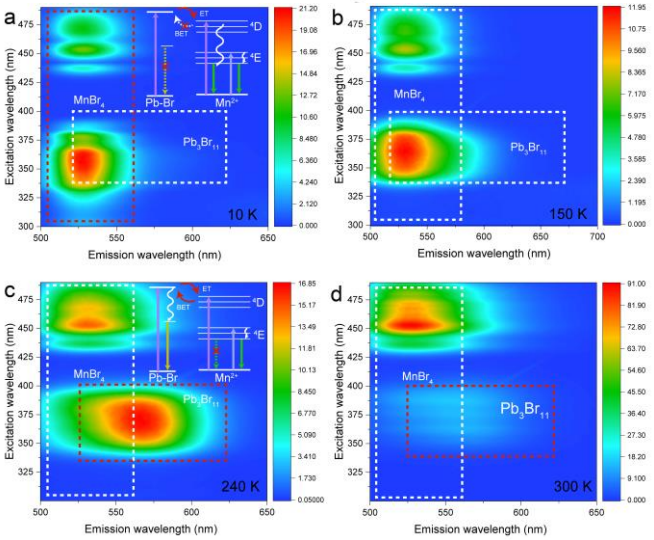

Figure 3. The consecutive PL/PLE correlation maps of $(C_9NH_{20})_9[Pb_3Br_{11}](MnBr_4)_2$ measured at 10K (a), 150 K (b), 240K (c) and 300K (d), respectively.

The temperature effect on the luminescence can be followed with the consecutive PL/PLE correlation maps measured at different temperatures (Figure 3). This experiment has been followed by the DSC measurement from 195 K to 300 K (Figure S6) to exclude the effect of structural phase transitions. At 10 K, the dominant emission and excitation are derived from Mn intra-atomic transitions (325-375 nm and 425-480 nm excitation, 525 nm emission) because the BET from $[MnBr_4]$ to $[Pb_3Br_{11}]$ is not activated (Figure 3a). As a result, excitons promoted to Mn ^{4}D states (325-375 nm excitation) remain there and relax non-radiatively to $^4T_1$ state, from which emission occurs (Figure 3a, inset). Figure S7 shows the PL decay curves of band 1 and band 2 at 80 K, and the lifetimes were calculated to be 418.23 μs and 410.35 μs, respectively. Nearly the same peak positions and decay curves of band 1 and band 2 further support that the luminescence is indeed only attributed to ^{4}D-to-$^6A_1$ transition of Mn^{2+}. At 240 K, the Mn ^{4}D excitation band starts to disappear and Pb_3Br_{11} excitation/emission band appears (Figure 3c). This is due to the activation of the BET from $[MnBr_4]$ to $[Pb_3Br_{11}]$ (Figure 3c, inset). The 425-480 nm excitation band remains intact as there is no close-lying lead bromide derived energy states and energy transfer processes don't occur. Moreover, the intensity of the band 1 relative to the band 2 decreases at 300 K (Figure 3d). This further corroborates that this band is derived from lead bromide states as emission intensity quenching with increasing temperature which is known for ns^2 emission centers.[13] The possibility of the energy transfer is supported by analyzing the density of states (DOS) calculated for $(C_9NH_{20})_9[Pb_3Br_{11}](MnBr_4)_2$ using DFT (Figure 4). For Pb_3Br_{11} cluster, Pb *s*-states and Br *p*-states contribute to the valence band minimum (VBM), while conduction band maximum (CBM) is formed by Pb *p*-states and Br *p*- and *s*-states. For the isolated $MnBr_4$ fragment, Mn *d*-states and Br *p*-states contribute to both VBM and CBM. Although

10.1002/ange.201911419

there is no hybridization between $MnBr_4$ and Pb_3Br_{11} states since they are localized on different fragments, they appear at similar energies, which is a predisposition for the energy transfer.

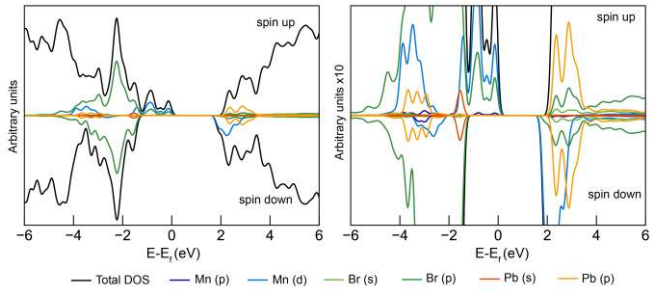

Figure 4. Density of states (DOS) plot for both spin-up and spin-down components. The y axis is multiplied ten-fold on the right figure.

Thus, all collected experimental data are consistent with the dual-emission mechanism that we proposed above. For band 1, when the temperature is relatively high, the sufficient thermal energy and relatively soft molecular environment stimulate the BET of carriers from the Mn^{2+} ^4D level to the ES of $[Pb_3Br_{11}]$,resulting in the quenched Mn^{2+} emission. Compared to the STE emission with the nanosecond lifetimes, Mn^{2+} emission has a much longer lifetime (up to milliseconds). Such long lifetimes favor the BET process, immensely compensating its anticipated inefficiency, eventually quenching the emission of Mn^{2+}. Thus only STE emission can be seen at room temperature. As the temperature decreases, the insufficient thermal energy and rigid molecular environment greatly restrict the process of BET. More carriers are captured by the ^4D level of Mn^{2+} and then transmit to $^6A_1$ level to yield characteristic green Mn^{2+} emission, which corresponds to the formation of two luminescent centers and the change in relative intensity ratios. Since BET is blocked at extremely low temperature, the states of $[Pb_3Br_{11}]$ are not populated which eventually caused the quenching of the emission from $[Pb_3Br_{11}]^{5-}$. As for band 2, insufficient excitation energy makes Mn^{2+} emission the only form of PL. Therefore, such a coexistence of STE and the ^4D to $^6A_1$ transition of Mn^{2+} in a single host provides a new way to achieve tunable emission in a single phase.

To verify that the room-temperature yellow emission of band 1 originates from STE, fs-TA spectroscopy by using a self-made femtosecond pump-probe setup is measured to monitor the direct signal of STE (Figure 5a), and the details can be also found in other references.[14] The photo-induced broadband absorption upon excitation at 367 nm is the typical characteristic of STE, which is different from the permanent defects with characteristic bleaching signal [10]. In that case we believe that permanent lattice defects do not contribute to the yellow emission of band 1. The formation time of STE manifests itself in the rise time of the observed induced absorption (Figure 5b). The ultrafast formation time (≈ 300 fs) shows no potential barrier from free carriers to STE. Moreover, the variation of the emission intensities excited at 375 nm and 450 nm as a function of the excitation power density were shown in Figure S8. As the excitation power increases, the intensity of band 1 increases linearly, while the band 2 increases first then tends to be saturated, and this result further verify the origins of the STE and ^4D to $^6A_1$ transition of Mn^{2+} ions for the 565 nm and 528 nm emission centers.[15] The model explaining the entirety of observed optical properties at room temperature is depicted in the Figure 5c, along with the sketch of the roles played by each of two building units (Figure 5d). Upon 365 nm excitation, lattice distortion in $[Pb_3Br_{11}]^{5-}$ clusters caused by the strong electron-phonon interactions will prompt the ultrafast formation of STE. The BET will be hindered at low temperatures as mentioned above, making ^4D-to-$^6A_1$ transition of Mn^{2+} the main emission channel. In contrast, STE cannot appear upon 450 nm excitation as the lack of excitation energy. The electron can only be excited to the ^4G-derived states of Mn^{2+} and then relaxed to the ^4D level, and the transmit from ^4D to $^6A_1$ level forming characteristic Mn^{2+} emission.

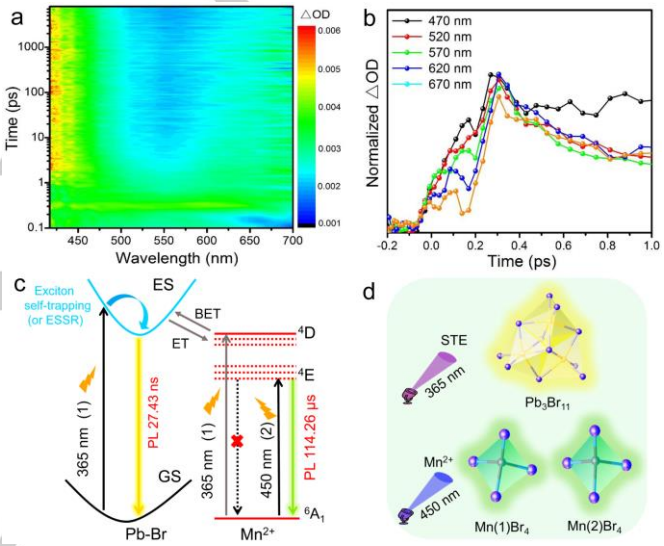

Figure 5. a) Contour plot of the fs-TA spectra of $(C_9NH_{20})_9[Pb_3Br_{11}](MnBr_4)_2$ upon photoexcitation at 368 nm with time window from 0 to 8000 ps. b) Normalized TA onsets probed at 470 nm, 520 nm, 570 nm and 620 nm. c) Diagram of luminescence processes in $(C_9NH_{20})_9[Pb_3Br_{11}](MnBr_4)_2$ at room temperature. (d) Luminescence model diagram of different illuminating centres at room temperature.

Since the stability of metal halides is crucial for their practical utility, their air stability (Figure S9), chemical stability (Figure S10), and thermal photoluminescence quenching behavior (Figure 6a) of $(C_9NH_{20})_9[Pb_3Br_{11}](MnBr_4)_2$ have been thoroughly tested. After exposing to air for 60 days or heating up to 523 K, no decomposition could be detected. Under 450 nm excitation, the temperature-dependent PL spectra of $(C_9NH_{20})_9[Pb_3Br_{11}](MnBr_4)_2$ from room temperature to 425 K with a temperature interval of 25 K were measured and the integrated emission intensity is about 78% at 375 K of the initial intensity at room temperature (the inset of Figure 6a). Owing to blue light-excitable green emission of $(C_9NH_{20})_9[Pb_3Br_{11}](MnBr_4)_2$, narrow FWHM (67 nm), as well as the good stability and high PLQY, this hybrid metal

halide makes for an attractive phosphor for WLEDs in the display applications. Thus, we fabricated WLEDs by combining green-emissive $(C_9NH_{20})_9[Pb_3Br_{11}](MnBr_4)_2$, the commercial red phosphor KSF:Mn^{4+} and the blue LED InGAN chips (λ = 455 nm), and Figure 6b shows the PL spectra of the WLED device under a current of 20 mA, and the inset shows the photographs of the fabricated WLED device. The obtained result reveals that the CIE color coordinate is (0.319, 0.372) with high luminous efficiency (LE) of 80.93 lm/W, color rendering index (CRI, R_a) of 79 and the white light correlated color temperature (*CCT*) of 6022 K. The PL spectra of the WLED device under various drive current are shown in Figure 6c. There is no apparent change in the curve shape, and the LE is as high as 70.11 lm/W and the CRI remains 77.5 when the current increases to 120 mA (Figure S11), suggesting the potential high-power application owing to the good stability. Moreover, color space (Figure 6d) of the as-fabricated WLEDs can reach 92.7% of the National Television System Committee standard (NTSC), which is close to that of WLEDs based on commercial green phosphor *β*-SiAlON:Eu^{2+}. The facile synthesis conditions, the narrowband green emitting (FWHM = 67 nm), the large color gamut, and the good thermal stability of the $(C_9NH_{20})_9[Pb_3Br_{11}](MnBr_4)_2$ indicate that this material has a promising application in WLEDs for advanced wide-color-gamut LCDs as also found other Mn based metal halides.[16] In addition, considering that $[Pb_3Br_{11}]^{5-}$ emitting species act as a yellow-emissive component, UV-pumped WLED was fabricated by combining a 365 nm near-UV LED chip with the mixture of blue ($BaMgAl_{10}O_{17}$:Eu^{2+} (BAM:Eu^{2+})), yellow ($(C_9NH_{20})_9[Pb_3Br_{11}](MnBr_4)_2$) and red (KSF:$Mn^{4+}$) phosphors, as presented in Figure S11. The *CCT*, R_a value and the CIE co-ordinate of the as obtained WLED are 5839 K, 93.7 and (0.326, 0.314), respectively. The above results indicate that by designing such an ultra-compact structure we have obtained a multifunctional material, which can be effectively excited at 365 nm and 450 nm and can be applied in both UV-pumped WLEDs and blue-light-pumped WLEDs.

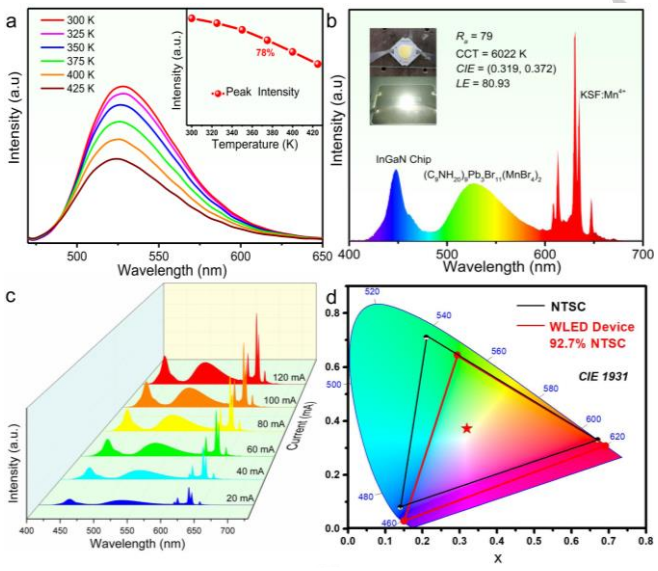

Figure 6. a) PL spectra (λ_{ex} = 450 nm) of $(C_9NH_{20})_9[Pb_3Br_{11}](MnBr_4)_2$ under different temperatures in the range of 300 – 425 K. The inset shows the comparison of PL intensities of $(C_9NH_{20})_9[Pb_3Br_{11}](MnBr_4)_2$ as a function of temperature. b) PL spectra of WLED fabricated by green phosphor $(C_9NH_{20})_9[Pb_3Br_{11}](MnBr_4)_2$, and commercial red phosphor KSF:Mn^{4+}on a 455 nm InGAN chip at 20 mA drive current. c) Drive current dependent PL spectra of fabricated WLED devices. d) CIE chromaticity diagram of $(C_9NH_{20})_9Pb_3Br_{11}(MnBr_4)_2$ of the fabricated WLED, color space of NTSC standard and WLED device.

In summary, we have designed and synthesized a novel 0D metal halide material $(C_9NH_{20})_9[Pb_3Br_{11}](MnBr_4)_2$, in which individual $[Pb_3Br_{11}]^{5-}$ clusters and $[MnBr_4]^{2-}$ tetrahedral units are co-crystallized with the large organic cation $C_9NH_{20}^+$. Seemingly intricate PL properties of this compound can be rationalized by the existence of two emitting centers corresponding to STE of $[Pb_3Br_{11}]^{5-}$ clusters and ^4D to $^6A_1$ transition of Mn^{2+} ions in $[MnBr_4]^{2-}$ tetrahedral units, whose populations are strongly dependent on the excitation wavelength and the temperature. $(C_9NH_{20})_9[Pb_3Br_{11}](MnBr_4)_2$ with excellent thermal stability, high PLQY and blue light excitable efficient luminescent property holds great potential in phosphor-converted LEDs, including the WLEDs backlights for LCDs. There results also motivate future discoveries of such cluster-assembled, luminescent metal halides. An important avenue in this regard will be to focus on non-heavy metal analogues with acceptable chemical durability; for instance, using other main group elements as STE -forming centers (Bi^{3+}, In^{3+}).

Acknowledgements

This work is supported by the National Natural Science Foundation of China (Nos. 51722202 and 51972118), Fundamental Research Funds for the Central Universities (D2190980), the Guangdong Provincial Science & Technology Project (2018A050506004) and by European Research Council (ERC) under the European Union's Horizon 2020 research and innovation programme (grant agreement No. [819740], project SCALE-HALO).

Keywords:0D materials • tunable emissions• light-emitting diodes

[1] a) P. F. Smet, J. J. Joos, *Nat. Mater.* **2017**, 16, 500-501; b) S. Pimputkar, J. S. Speck, S. P. DenBaars, S. Nakamura, *Nat. Photonics* **2009**, 3, 180; c) H. X. Liao, M. Zhao, Y. Y. Zhou, M. S. Molokeev, Q. L. Liu, Q. Y. Zhang, Z. G. Xia, *Adv. Funct. Mater.* **2019**, 1901988.

[2] a) Z. G. Xia, Z. H. Xu, M. Y. Chen, Q. L. Liu, *Dalton Trans.* **2016**, 45, 11214-11232; b) H. A. Hoppe, *Angew. Chem.* **2009**, 48, 3572-3582.

[3] a) Z. K. Tan, R. S. Moghaddam, M. L. Lai, P. Docampo, R. Higler, F. Deschler, M. Price, A. Sadhanala, L. M. Pazos, D. Credgington, F. Hanusch, T. Bein, H. J. Snaith, R. H. Friend, *Nat. Nanotechnol.* **2014**, 9 (9), 687-692. b) Y. Zhao, K. Zhu, *Chem. Soc. Rev.* **2016**, 45 (3), 655-689. c) M. Ahmadi, T. Wu, B. Hu, *Adv. Mater.* **2017**, 29 (41), 1605242. d) M. V. Kovalenko, L. Protesescu, M. I. J. S.

Bodnarchuk, *Science*. **2017**, *358*, 745-750. d) S. Yakunin, B. M. Benin, Y. Shynkarenko, O. Nazarenko, M. I. Bodnarchuk, D. N. Dirin, C. Hofer, S. Cattaneo, M. V. Kovalenko, *Nat. Mater.* **2019**, *18*, 846-852.

[4] a) Y.Y. Li, W.J. Wang, H. Wang, H. Lin, L.M. Wu, *Cryst. Growth. Des.* **2019**, 19, 4172-4192; b) H. Kageyama, K. Hayashi, K. Maeda, J. P. Attfield, Z. Hiroi, J. M. Rondinelli, K. R. Poeppelmeier, *Nat. Commun.* **2018**, 9, 772; c) J. Z. Chen, Y. G. Rong, A. Mei, Y. L. Xiong, T. F. Liu, Y. S. Sheng, P. Jiang, L. Hong, Y. Guan, X. T. Zhu, X. M. Hou, M. Duan, J. Q. Zhao, X. Li, H. W. Han, *Adv. Energy. Mater.* **2016**, 6. (5), 1502009. d) K. Chen, L. Li, *Adv. Mater.* **2019**, 1901115.

[5] H. R. Lin, C. K. Zhou, Y. Tian, T. Siegrist, B. W. Ma, *ACS Energy Letters* **2017**, 3, 54-62.

[6] a) V. Morad, Y. Shynkarenko, S. Yakunin, A. Brumberg, R. D. Schaller, M. V. Kovalenko, *J. Am. Chem. Soc.* **2019**, *141*, 9764-9768. b) M. I. Saidaminov, J. Almutlaq, S. Sarmah, I. Dursun, A. A. Zhumekenov, R. Begum, J. Pan, N. Cho, O. F. Mohammed, O. M. Bakr, *ACS Energy Letters* **2016**, *1*, 840-845. c) C. Zhou, H. Lin, H. Shi, Y. Tian, C. Pak, M. Shatruk, Y. Zhou, P. Djurovich, M. H. Du, B. Ma, *Angew Chem Int Ed Engl* **2018**, *57*, 1021-1024.d) C. Zhou, H. Lin, M. Worku, J. Neu, Y. Zhou, Y. Tian, S. Lee, P. Djurovich, T. Siegrist, B. Ma, *J. Am. Chem. Soc.* **2018**, *140*, 13181-13184.

[7] a) R. L. Zhang, X. Mao, Y. Yang, S. Q. Yang, W. Y. Zhao, T. Wumaier, D. H. Wei, W. Q. Deng, K. L. Han, *Angew. Chem.* **2019**, 58, 2725-2729; b) C. K. Zhou, H. R. Lin, J. Neu, Y. Zhou, M. Chaaban, S. Lee, M. Worku, B. Chen, R. Clark, W. B. Cheng, J. J. Guan, P. Djurovich, D. Z. Zhang, X. J. Lü, J. Bullock, C. Pak, M. Shatruk, M. H. Du, T. Siegrist, B. W. Ma, *ACS Energy Letters* **2019**, 4, 1579-1583.

[8] a) M. Iwanaga, J. Azuma, M. Shirai, K. Tanaka, T. Hayashi, *Phys. Rev. B* **2002**, 65, 214306; b) M. D. Smith, A. Jaffe, E. R. Dohner, A. M. Lindenberg, H. I. Karunadasa, *Chem. Sci.* **2017**, 8, 4497-4504; c) T. Hu, M. D. Smith, E. R. Dohner, M. J. Sher, X. Wu, M. T. Trinh, A. Fisher, J. Corbett, X. Y. Zhu, H. I. Karunadasa, A. M. Lindenberg, *J. Phys. Chem. Lett.* **2016**, 7, 2258-2263. d)T. Jun, K. Sim, S. Iimura, M. Sasase, H. Kamioka, J. Kim, H. Hosono, *Adv. Mater.* **2018**, *30*, e1804547.

[9] a)Y. Rodríguez-Lazcano, L. Nataf, F. Rodríguez, *Phys. Rev. B* **2009**, 80, 085115. b) M. Li, J. Zhou, M. S. Molokeev, X. Jiang, Z. Lin, J. Zhao, Z. Xia, *Inorg. Chem.* **2019**, 58, 13464-13470.

[10] J. Zhou, M. Z. Li, L. X. Ning, R. L. Zhang, M. S. Molokeev, J. Zhao, S. Q. Yang, K. L. Han, Z. G. Xia, *J. Phys. Chem. Lett.* **2019**, 10, 1337-1341.

[11] a) C. Jiang, N. Zhong, C. Luo, H. Lin, Y. Zhang, H. Peng, C. G. Duan, *Chem. Commun.* **2017**, 53, 5954-5957; b) Y. Zhang, W. Q. Liao, D. W. Fu, H. Y. Ye, Z. N. Chen, R. G. Xiong, *J. Am. Chem. Soc.* **2015**, 137, 4928-4931.

[12] a) R. Beaulac, P. I. Archer, J. van Rijssel, A. Meijerink, D. R. J. N. I. Gamelin, *Nano Lett.* **2008**, *8*, 2949-2953; b) W. J. Mir, Y. Mahor, A. Lohar, M. Jagadeeswararao, S. Das, S. Mahamuni, A. Nag, *Chem. Mater.* **2018**, *30*, 8170-8178.

[13] a) P.W.M.Jacobs, *J. Phys. Chem. Solids* **1991**, *52*, 35-67. b) K. M. McCall, C. C. Stoumpos, S. S. Kostina, M. G. Kanatzidis, B. W. Wessels, *Chem. Mater.* **2017**, *29*, 4129-4145.

[14] a) S. Q. Yang, Y. Zhang, K. L. Han, *J. Lumin.* **2019**, 206, 46-52; b) S. Q. Yang, K. L. Han, *J Phys. Chem A.* **2016**, 120, 4961-4965.

[15] T. Schmidt, K. Lischka, W. Zulehner, *Phys. Rev. B* **1992**, 45, 8989-8994.

[16] a) L. J. Xu, C. Z. Sun, H. Xiao, Y. Wu, Z. N. Chen, *Adv Mater* **2017**, *29,1605739.* b) B. Su, M. S. Molokeev, Z. Xia, *J. Mater. Chem. C*, **2019**, 7(36): 11220-11226.

10.1002/ange.201911419

WILEY-VCH

Entry for the Table of Contents

RESEARCH ARTICLE

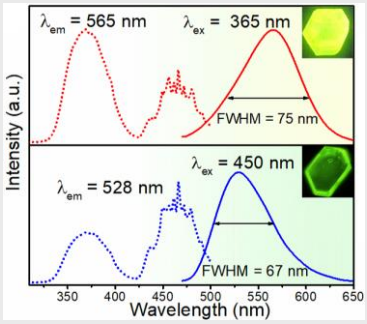

*Mingze Li, Jun Zhou, Guojun Zhou, Maxim S. Molokeev, Jing Zhao, Viktoriia Morad, Maksym V. Kovalenko and Zhiguo Xia**

Page No. – Page No.

Hybrid Metal Halides with Multiple Photoluminescence Centers

We report on a novel 0D metal halide material $(C_9NH_{20})_9[Pb_3Br_{11}](MnBr_4)_2$, with two distinct emitting centers - self-trapped excitons residing on $[Pb_3Br_{11}]^{5-}$ clusters and ^4D-to-$^6A_1$ transitions of Mn^{2+} ions in $[MnBr_4]^{2-}$ tetrahedral units. This is the first example of Mn^{2+} emission and STE emission coexisting in a single crystalline material, and the tunable emission is strongly dependent on the excitation wavelength and the temperature. Furthermore, the highly stable performance upon light and heat and high PLQY under 450 nm blue light excitation show its potential in backlight display application. This family of hybrid metal halides with mixed and isolated polyhedron units could act as an effective way to achieve tunable emissions and modulate the properties required in optoelectronic devices.